GCN5 restricts PRX-dependent lignin deposition during salt stress in Arabidopsis

Mansi Sharma[1,2], Jan Masood[3,4], Pavel Kerchev[3,5], Iva Mozgova[1,2], Michael Wrzaczek[1,2*]

[1]Institute of Plant Molecular Biology, Biology Centre, Czech Academy of Sciences, 37005 České Budějovice, Czech Republic

[2]Faculty of Science, University of South Bohemia, 37005 České Budějovice, Czech Republic

[3]Mendel University in Brno, 613 00 Brno, Czech Republic

[4]Current address: Horticultural Sciences Department, University of Florida, Gainesville, FL, USA, 32611

[5]Current address: Estación Experimental del Zaidín (EEZ-CSIC), 18008, Granada, Spain

[*]Corresponding author: Michael Wrzaczek (michael.wrzaczek@umbr.cas.cz)

Abstract

Histone acetylation shapes transcriptional programs during environmental stress. The Arabidopsis histone acetyltransferase *GCN5/HAG1*, a catalytic subunit of the SAGA complex, has been implicated in salt stress responses and cell wall integrity. Here, we show that loss of *GCN5* enhances reactive oxygen species (ROS) accumulation under NaCl stress and is accompanied by altered expression of class III peroxidase genes, with strong salt-induced upregulation of *PRX71* and elevated basal *PRX33* transcript abundance. Consistent with a role for these peroxidases in stress-associated cell wall remodeling, overexpression of *PRX71* or *PRX33* in the wild-type is sufficient to promote ectopic lignin deposition in roots. Conversely, *prx71* and *prx33* mutants show improved growth under salt stress and on the cellulose biosynthesis inhibitor isoxaben, and they lack the pronounced ectopic root lignification observed in *gcn5* under salt stress. Chromatin immunoprecipitation followed by qPCR (ChIP-qPCR) reveals reduced H3K9 acetylation at *PRX71* and *PRX33* promoter regions in *gcn5* compared with the wild-type, and reduced transcript abundance of candidate upstream transcription factors (TFs), including *GATA21* and *MYBS2*, accompanied by reduced H3K9ac at their loci. Together, our results support a model in which GCN5 constrains *PRX71/PRX33*-mediated lignification during stress, likely through an indirect regulatory route that integrates chromatin state and transcription factor activity to limit stress-associated lignification while maintaining root growth under salt stress.

Keywords

Arabidopsis thaliana; *GCN5/HAG1*; histone acetylation; H3K9ac; salt stress; cell wall integrity; lignification; class III peroxidase; reactive oxygen species

Introduction

Plants are constantly exposed to abiotic and biotic stresses that can occur alone or in combination, requiring rapid signaling as well as longer-term acclimation (Wurzinger, Mair, Pfister & Teige 2011; Boudsocq & Sheen 2013). Among the earliest responses are changes in cytosolic calcium levels and the production of reactive oxygen species (ROS), which act as signaling molecules (Wurzinger *et al.* 2011; Boudsocq & Sheen 2013). Stress also activates mitogen-activated protein kinase (MAPK) and hormone signaling networks (Mittler 2002; Baxter, Mittler & Suzuki 2014; Xia *et al.* 2015; Jalmi & Sinha 2015). Among these stresses, salt stress is a major abiotic constraint because it imposes an early osmotic limitation on growth and a later ionic phase that can exacerbate cellular damage (Munns & Tester 2008). Plants rapidly respond to biotic and abiotic stimuli by triggering responses that involve changes to gene transcription, inherently connected to changes in chromatin structure, and can also orchestrate rapid but also long-lasting epigenetic changes in response to stress. These changes, including histone modifications, are inducible within minutes to hours but can persist for days after the initial stimulus and gradually fade, depending on the locus and stress regime (Ding, Fromm & Avramova 2012; Lämke & Bäurle 2017; Ma, Xing, Li & Jiang 2025). Chromatin structure is determined by combinations of histone modifications including acetylation, methylation, phosphorylation, ubiquitylation, and sumoylation and others, as well as by DNA methylation, which together regulate gene expression without altering the DNA sequence.

Among these modifications, histone acetylation plays a key role in modulating chromatin accessibility. Histone acetylation status is balanced by the activities of histone acetyltransferases (HATs) and histone deacetylases (HDACs), and can be modulated under stress conditions (Ueda & Seki 2020). This balance can be altered, for example, treatment with the HDAC inhibitor Ky-2 increases histone acetylation in *Arabidopsis thaliana* under salt stress, leading to increased expression of salt-responsive genes and contributing to improved salt tolerance (Sako *et al.* 2016). Similarly, MSI1 (WD40-repeat histone binding protein), which forms a complex with HDA19 that deacetylates H3K9 at the abscisic acid (ABA) receptor genes, represses their expression. Loss of MSI1 or HDA19 results in increased ABA sensitivity and enhances tolerance to salt stress in *Arabidopsis* (Mehdi *et al.* 2016). Together, these studies illustrate that modulating histone acetylation plays a key role in controlling stress-responsive gene expression and stress tolerance in plants. One well-characterized HAT module subunit is GCN5 (General Control Non-repressed Protein 5), which is part of the SAGA (Spt–Ada–Gcn5 acetyltransferase) complex, a conserved transcriptional coactivator in eukaryotes

that influences a wide range of cellular processes by modulating histones through acetylation and deubiquitination (Moraga & Aquea 2015). In addition to GCN5, SAGA comprises the subunits along with Alteration/Deficiency in Activation 2B (ADA2B), Alteration/Deficiency in Activation 3 (ADA3), SGF29 (SAGA-associated factor 29) subunits (Moraga & Aquea 2015). The catalytic HAT subunit GCN5 acetylates specific lysines on histone H3 at positions K9, K14, K27, and of histone H4 at position K12, and it is crucial for regulating the expression of genes involved in plant development and stress responses (Benhamed, Bertrand, Servet & Zhou 2006; Servet, Conde E Silva & Zhou 2010; Hu *et al.* 2015; Zheng *et al.* 2019; Kim *et al.* 2020). Importantly, GCN5 is involved in salt stress tolerance and cell-wall integrity by modulating H3K9 and H3K14 acetylation linked to the activation of chitinase-like-1 (*CTL1*), polygalacturonase involved in expansion-3 (*PGX3*), and MYB domain protein 54 (*MYB54*) genes associated with cellulose synthesis. This affects turgor, growth dynamics, and cell wall integrity, whereby plants actively remodel cell wall polymers to maintain growth and survival (Zheng *et al.* 2019).

In addition to the SAGA complex, plants have recently been reported to also contain a PAGA (Plant-ADA2A-GCN5-acetyltransferase) complex that influences the transcription of hormone-related genes, controlling plant growth traits such as height and branching (Wu *et al.* 2023). Both SAGA and PAGA share the GCN5 HAT subunit, but the SAGA complex contains ADA2B, while PAGA contains ADA2A. The two complexes independently generate different levels of acetylation, facilitating transcriptional activation (Wu *et al.* 2023).

A key aspect of plant growth and environmental response is the continuous modification of the cell wall, which is loosened by enzymes such as expansins and xyloglucan endotransglucosylase/hydrolase (XTHs) to enable cell expansion. The plant cell wall acts as the plant's first line of defense against stress during pathogen attack and responds to osmotic or salt stress, and undergoes remodeling to maintain integrity and prevent collapse leading to restricted plant growth (Tenhaken 2015; Cosgrove 2016; Tariq, Ma & Zhao 2025). The plant cell wall consists of cellulose, hemicellulose, and pectin, with cellulose forming long, unbranched chains of β-1,4-linked glucose units (Somerville *et al.* 2004), synthesized by cellulose synthase (CESA) proteins (Cosgrove 2005; Gutierrez, Lindeboom, Paredez, Emons & Ehrhardt 2009). Loss of function or chemical inhibition of CESA by compounds such as by isoxaben or thaxtomin A, disrupts cellulose biosynthesis and cell wall integrity, which results in an ectopic lignin deposition (Caño-Delgado, Penfield, Smith, Catley & Bevan 2003; Persson *et al.* 2007; Bischoff, Cookson, Wu & Scheible 2009). In addition to its ectopic deposition

105 under stress, lignin is normally deposited in the secondary cell wall, strengthening the tissue,
106 making the wall less permeable to water and facilitating water transport through the xylem
107 (Rogers & Campbell 2004; Boyce *et al.* 2004). Abiotic and biotic stresses can modulate the
108 expression of lignin biosynthesis genes. In *Arabidopsis* under salt stress, lignin accumulation
109 is accompanied by higher expression of lignin biosynthesis genes (Moura, Bonine, De Oliveira
110 Fernandes Viana, Dornelas & Mazzafera 2010; Chun *et al.* 2019). The stress-induced lignin
111 deposits occur as a secondary cell wall remodeling response mediated by Class III peroxidases
112 (PRXs), which comprise 73 isoforms in *Arabidopsis* that use H_2O_2 to oxidize monolignols,
113 leading to lignin formation (Passardi, Penel & Dunand 2004; Marjamaa, Kukkola & Fagerstedt
114 2009; Bischoff *et al.* 2009). Specific PRXs, including *PRX2*, *PRX25*, and *PRX71*, contribute to
115 stem lignification, with mutants showing reduced lignin without developmental defects
116 (Shigeto, Kiyonaga, Fujita, Kondo & Tsutsumi 2013). *PRX71* also plays a role in reinforcing
117 the cell wall, which helps limit cell expansion, and is upregulated in plants with altered pectin
118 or after cellulose synthesis inhibition, promoting ROS accumulation and influencing growth
119 (Raggi *et al.* 2015), while knockdown of *PRX33* and *PRX34* reduces MAMP-induced defense
120 proteins, lowers apoplastic ROS production, and alters cell wall remodeling enzymes (Daudi
121 *et al.* 2012; O'Brien *et al.* 2012). Together, these observations place peroxidase-driven ROS
122 and lignification at the intersection of stress signaling and cell wall remodeling. Yet it remains
123 unclear how the PRX gene expression is tuned at the chromatin-level during salt stress.

124 Here, we investigate how GCN5 influences the expression of two class III peroxidases, *PRX71*
125 and *PRX33*, and how this relates to ROS accumulation and lignin deposition during salt stress.
126 Using T-DNA insertion mutants and *PRX71* and *PRX33* overexpressing lines, histochemical
127 assays, gene expression analyses, and ChIP-qPCR, we identified an association between
128 GCN5-dependent acetylation and a transcriptional network that constrains peroxidase-linked
129 lignification in stressed seedlings. By connecting a chromatin regulator (GCN5) to distinct
130 PRX loci and downstream cell wall phenotypes, this work extends our understanding of how
131 epigenetic control helps balance stress protection with growth in salt-challenged seedlings.

132

Materials and Methods

Plant material and growth conditions

Arabidopsis thaliana T-DNA insertion line *gcn5* (*SALK_048427*) was obtained from the Arabidopsis Biological Resource Centre (ABRC). The T-DNA insertion lines *prx71-1* (*SALK_123643C*), *prx71-2* (*SALK_121202C*), and *prx33* (*SALK_062314C*) were obtained from the Nottingham Arabidopsis Stock Centre (NASC) (Alonso *et al.* 2003). All mutants are in the Columbia-0 (Col-0) background, and Col-0 was used as the wild-type control for all experiments. Primers used in this study are listed in Table S1.

For genotyping, genomic DNA was prepared directly from seedling tissue and PCR was performed using Phire™ Plant Direct PCR Master Mix (Thermo Scientific, F130WH) following the manufacturer's instructions. Insertion genotypes were confirmed by PCR (Supplementary Figure S4a). For transcript verification of insertion lines, semi-quantitative RT-PCR was performed using total RNA isolated from 10-day-old seedlings, and first-strand cDNA was synthesized as described by (Colina, Krasensky-Wrzaczek, Pérez-Guillén & Wrzaczek 2026). Expression was normalized to the reference gene (*PP2AA3*) (Supplementary Figure S4b).

Seeds were surface sterilized in 70% (v/v) ethanol containing 0.02% (v/v) Triton X-100 for 5 min, followed by 1 min in 96% (v/v) ethanol and five rinses in sterile water. Seeds were plated on half-strength Murashige and Skoog (MS) medium (Duchefa, M0222.0050) adjusted to pH 5.8 and supplemented with 0.8% (w/v) agar and 0.05% (w/v) MES unless stated otherwise. After 2 days of stratification in the dark at 4 °C, plates were transferred to a growth chamber maintained at 22 °C under a 16 h light/8 h dark photoperiod (light intensity 128.26 µmol m-2 s-1). All treatments were performed using sodium chloride (P- Lab, Q09101) and isoxaben (Merck, 36138), unless otherwise indicated.

Plasmid construction and plant transformation

PRX71 and *PRX33* overexpression constructs were generated using MultiSite Gateway cloning (Invitrogen; Thermo Fisher Scientific). The coding sequences (CDS) of *PRX71* (984 bp) and *PRX33* (1,062 bp) were amplified from Arabidopsis cDNA. PCR products were recombined into pDONR221 using BP Clonase II enzyme mix (Invitrogen), yielding entry clones carrying *PRX71* or *PRX33* CDS.

For expression in plants, an LR recombination reaction was performed using LR Clonase II Plus enzyme mix (Invitrogen) to assemble the *CaMV 35S* promoter, an mVenus YFP tag, and

165 the *PRX* CDS fragments into the destination vector *pBm43GW* (Karimi, De Meyer & Hilson
166 2005). The resulting constructs (*35S::PRX71-YFP* and *35S::PRX33-YFP*) were introduced into
167 *Agrobacterium tumefaciens* strain GV3101 (pSoup) (Lifeasible) and transformed into Col-0
168 plants by floral dip. T1 plants were used for all subsequent experiments.

169 **Histochemical detection of ROS accumulation**

170 Reactive oxygen species accumulation was assessed using 3,3′-diaminobenzidine (DAB)
171 staining. Ten-day-old seedlings were treated with 0 mM or 150 mM NaCl or 300 nM isoxaben
172 on half-strength liquid MS medium for 6 hours. Seedlings were then infiltrated with 0.1% (w/v)
173 DAB (Sigma-Aldrich, D5637) dissolved in 10 mM MES buffer (pH 6.5) until fully saturated
174 and incubated for 40 min under light. After staining, seedlings were rinsed with water and
175 chlorophyll was removed by incubation in 100% ethanol overnight. Samples were stored in
176 water until imaging. Images were acquired using an Olympus SZ16 stereomicroscope equipped
177 with a PROMICAM 2-5CP digital camera.

178 **Histochemical detection of lignin deposition**

179 Lignin deposition in roots was assessed by phloroglucinol–HCl staining. Two-weeks-old
180 seedlings were treated with 0 mM or 150 mM NaCl on half-strength liquid MS medium for 6
181 hours. Roots were stained with 1% (w/v) phloroglucinol–HCl (Sigma-Aldrich, P3502) for 10
182 min at room temperature. Stained samples were imaged immediately using an Olympus
183 MacroView MVX10 stereomicroscope.

184 **Root growth assays**

185 For root length measurements, seedlings were grown vertically on half-strength MS medium
186 for 5 days and then transferred to one of the following media: control (0 mM NaCl), 150 mM
187 NaCl, or 2.5 nM isoxaben. Plates were returned to vertical orientation, and seedlings were
188 grown for an additional 7 days. Primary root lengths were measured at the endpoint (day 12).
189 Each treatment was performed using at least three independent biological replicates.

190 **Survival rate analysis**

191 For salt survival assays, 5-day-old seedlings were transferred to half-strength MS medium
192 containing 0 mM or 150 mM NaCl and grown for 7 days. Survival was determined as the
193 percentage of seedlings that remained green and viable relative to the total number of
194 transferred seedlings. Each treatment included at least three biological replicates.

195 **RNA extraction and quantitative real-time PCR (qRT–PCR)**

196 For gene expression analyses, seedlings were grown on half-strength MS medium (pH 5.8)
197 without sucrose for 10 days. Salt treatments were performed by transferring seedlings to liquid
198 MS medium containing 150 mM NaCl, and tissue was harvested at 0, 3, 6, and 12 hours after
199 treatment. Samples were immediately frozen in liquid nitrogen and homogenized with glass
200 beads using a bead mill. Total RNA was extracted using ROTIZOL (Karl Roth, 9319.2)
201 according to the manufacturer's instructions, following the workflow described by (Colina *et*
202 *al.* 2026). RNA was treated with DNase I to remove genomic DNA contamination as described
203 by (Colina *et al.* 2026). First-strand cDNA was synthesized from 1 µg DNase-treated RNA
204 using the RevertAid cDNA Synthesis Kit (Thermo Fisher Scientific, K1621) with oligo(dT)
205 primers.

206 Quantitative real-time PCR was performed using gene-specific primers (Supplementary Table
207 S1) with DBdirect PCR SYBR Mix SuperSens (DIANA Biotechnologies, DB-1274).
208 Amplification was measured with a thermocycler (Bio-Rad, CFX Connect Real-Time PCR
209 Detection System). Expression was normalized to the housekeeping gene (*PP2AA3*), following
210 (Czechowski, Stitt, Altmann, Udvardi & Scheible 2005). Relative expression levels were
211 calculated using the ΔΔCT method. Each condition was measured using three independent
212 biological replicates and two technical replicates per biological replicate.

213 **Chromatin immunoprecipitation (ChIP) and ChIP–qPCR**

214 ChIP was performed using a crosslinked Arabidopsis ChIP protocol adapted from (Mozgová
215 *et al.* 2015). Wild-type (Col-0) and gcn5 seedlings were grown on half-strength MS plates for
216 10 days and treated in liquid half-strength MS with 150 mM NaCl for 3 hours; control samples
217 were mock-treated without NaCl. Tissue (~100 mg) was crosslinked in 1% formaldehyde by
218 vacuum infiltration (10 min) and quenched with 0.125 M glycine (5 min). Samples were
219 washed, snap-frozen, and ground in liquid nitrogen. Nuclei were extracted in Modified
220 Extraction Buffer, filtered through Miracloth, and pelleted (1500 rcf, 10 min, 4 °C). Nuclei
221 were lysed in 1% SDS and chromatin was fragmented by sonication (Diagenode Bioruptor 300,
222 7 cycles, 30 s ON/30 s OFF, high power) to obtain ~0.3–1.5 kb fragments, then diluted with
223 ChIP dilution buffer to reduce SDS to 0.1% and cleared by centrifugation. Ten percent of each
224 sample was saved as input DNA. Immunoprecipitation was performed overnight at 4 °C with
225 rotation using anti-H3K9ac (Sigma-Aldrich, 07-352) and, where indicated, total H3 (Sigma-
226 Aldrich, 07-690) and IgG (Sigma-Aldrich, R2655) as a negative control. Immune complexes
227 were captured using Protein A magnetic beads and washed using low- and high-salt wash
228 buffers. Chromatin was eluted twice (elution buffer; 65 °C, 15 min) and crosslinks were

229 reversed by NaCl addition and incubation at 65 °C for ≥6 hours. Samples were treated with
230 proteinase K (45 °C, 1 hour), and DNA was purified using the IPure kit v2 (Diagenode,
231 C03010015).

232 ChIP qPCR was done using DBdirect PCR SYBR Mix SuperSens (DIANA Biotechnologies,
233 DB-1274), and measured with a thermocycler (Bio-Rad, CFX Connect Real-Time PCR
234 Detection System). ChIP enrichment was quantified by qPCR using three biological replicates,
235 with two technical replicates per biological replicate. Enrichment was calculated relative to
236 input DNA and normalized to total H3. A transposable element locus (*At4g03770*) was used as
237 an H3K9ac negative control locus.

238 **Statistical analysis**

239 All statistical analyses were performed in R (2023-12-1; Build 402; Posit Software) using
240 RStudio (2024-04-24, 4.4.0; R Foundation). Data were initially tested for normality and
241 homogeneity of variances. Levene's test and F-test were applied to assess variance
242 homogeneity. For datasets meeting parametric assumptions, *t*-tests, and two-way ANOVA
243 were used, with Tukey's post-hoc test applied for multiple pairwise comparisons. For datasets
244 that did not meet parametric assumptions, Kruskal–Wallis tests were used as a non-parametric
245 alternative followed by wilcoxon post-hoc test for pairwise comparisons. In all analyses, $p <$
246 0.05 was considered significant.

247 **Results**

248 **Loss of GCN5 increases ROS accumulation and alters *PRX33* and *PRX71* expression**
249 **during salt stress**

250 To confirm and extend the previous reports that *gcn5* is sensitive to salt stress (Zheng *et al.*
251 2019), we analyzed the survival rate and root growth of *gcn5* seedlings under 150 mM NaCl.
252 We included *gcn5* mutants, wild-type plants, and three independent complementation lines
253 expressing *pGCN5::GCN5-GFP* in *gcn5* mutant background (described in De Smet *et al.* 2025)
254 to confirm that the observed phenotypes were specifically caused by the loss of GCN5. Survival
255 rates and primary root lengths of plants grown on 150 mM NaCl were measured on day 12 and
256 normalized to control conditions (Figure S1a, b). The *gcn5* mutant showed reduced survival
257 (Figure S1a) and shorter primary root length (survival rate, Figure S1a; root length, (Figure
258 S1b) compared with wild-type. All three complementation lines partially rescued the survival
259 phenotype (Figure S1a) and restored root length to levels similar to the wild type (Figure S1b).

260 Thus, consistent with previous findings (Zheng *et al.* 2019), we observed that the *gcn5* mutant
261 analyzed in this study was sensitive to salt stress.

262 Salt stress induces ROS accumulation (Mittler 2002) and GCN5 may play a role in maintaining
263 ROS balance under salt stress. TaHAG1, a wheat ortholog of GCN5, contributes to ROS
264 balance under salt stress (Zheng *et al.* 2021). We next investigated whether the loss of GCN5
265 affects ROS accumulation in *Arabidopsis.* To examine this, we performed DAB staining to
266 visualize hydrogen peroxide (H_2O_2) accumulation in 10-day-old *gcn5* and wild-type plants
267 following 6 hours of treatment with 150 mM NaCl or 300 nM isoxaben, both of which can
268 trigger ROS accumulation. Isoxaben triggers a wide spectrum of cell wall integrity-related
269 adaptations, including hormone signaling and lignin accumulation, by disrupting cellulose
270 biosynthesis (Scheible, Eshed, Richmond, Delmer & Somerville 2001; Denness *et al.* 2011;
271 Hamann 2015). Under mock conditions, ROS accumulation was not detectable in either wild-
272 type plants or the *gcn5* mutant. However, in response to NaCl and isoxaben treatments, ROS
273 accumulation was enhanced in the *gcn5* mutant compared with wild-type (Figure 1a).

274 To explore the molecular basis of the elevated ROS accumulation in *gcn5* under stress
275 conditions, we analyzed publicly available transcriptomic data to identify genes differentially
276 expressed in the *gcn5* mutant (Wu *et al.* 2023). In this dataset, 23 peroxidase genes were
277 misregulated in the *gcn5* mutant, of which 20 were upregulated and 3 downregulated (Figure
278 S1c). Since the enhanced salt sensitivity of the *gcn5* plants was previously connected with
279 altered cell wall synthesis and enhanced lignin deposition (Zheng *et al.* 2019), we focused on
280 class III PRXs involved in lignin polymerization (Cosio & Dunand 2009). The upregulation of
281 class III PRX transcripts in *gcn5* could influence ROS balance, as they utilize H_2O_2 during
282 lignin polymerization. We hypothesized that the increased expression of these PRX genes in
283 the *gcn5* mutant contributes to lignin deposition, as lignin is known to accumulate in response
284 to cell wall damage (Passardi *et al.* 2004; Denness *et al.* 2011). Based on this, *PRX2*, *PRX25*,
285 *PRX71*, and *PRX52* were selected for their reported roles in lignification (Shigeto *et al.* 2013;
286 Fernández-Pérez, Pomar, Pedreño & Novo-Uzal 2015; Shigeto & Tsutsumi 2016). In addition,
287 *PRX33* was included based on its reported involvement in ROS-related responses (Daudi *et al.*
288 2012; Arnaud *et al.* 2017), in line with the observed ROS accumulation in the *gcn5* mutant.

289 Transcript abundance of these selected PRX genes were quantified by qRT-PCR at different
290 time points after treatment with 150 mM NaCl in wild type and *gcn5* (Figure S1d). Among
291 them, *PRX71* and *PRX33* showed consistently higher expression in *gcn5* compared to wild-

292 type plants. *PRX33* was elevated in *gcn5* under control conditions but showed a weaker
293 induction upon salt treatment compared to wild type. By contrast, *PRX71* transcript abundance
294 increased after 6 hours of NaCl treatment and continued to rise up to 12 hours, reaching levels
295 significantly higher than those in wild type (Figure 1b). Overall, this indicates that *PRX33* and
296 *PRX71* are upregulated in the *gcn5* mutant and were therefore selected for subsequent
297 functional analyses.

298 ***PRX71* and *PRX33* overexpression alters lignin deposition**

299 To test whether the upregulation of these PRX genes is sufficient to promote lignin deposition,
300 we next examined *PRX71* and *PRX33* overexpression lines together with the *prx33*, *prx71*, and
301 *gcn5* mutant lines. Based on our observation that the loss of GCN5 resulted in enhanced *PRX71*
302 and *PRX33* expression and the known involvement of class III PRXs in lignin polymerization,
303 we next investigated whether upregulation of *PRX71* and *PRX33* contributes to enhanced lignin
304 deposition and potentially to maintaining cell wall integrity. To visualize lignin, we used
305 phloroglucinol-HCl staining, which reacts with the aldehyde group of lignin and results in a
306 pink coloration (Davidson *et al.* 1995; Pradhan Mitra & Loqué 2014). The *gcn5* mutant
307 displayed increased lignin deposition in the vasculature compared with wild-type roots,
308 whereas *prx71* and *prx33* resembled wild-type roots. *PRX71* and *PRX33* overexpression lines
309 showed enhanced lignin deposition in the vasculature, similar to *gcn5,* but in addition displayed
310 ectopic lignin accumulation (Figure 2). These results indicate that elevated PRX expression is
311 sufficient to promote vascular and ectopic lignin deposition, recapitulating key aspects of the
312 *gcn5* phenotype, independent of GCN5 loss.

313 Given these observations and because GCN5 loss leads to reduced cellulose content, as it
314 regulates cellulose synthesis genes (Zheng *et al.* 2019), increased lignin deposition could serve
315 as a compensatory reinforcement mechanism to maintain cell wall strength. Consistent with
316 this idea, our findings indicate that *PRX71* and *PRX33*, also upregulated in *gcn5*, promote
317 vascular and ectopic lignin deposition, which may help to counteract cell wall disruption.

318 **Altered lignin deposition and root length responses under salt stress**

319 Considering the increased lignin deposition in both *gcn5* and PRX overexpression lines, we
320 next asked how these changes relate to salt-driven root growth phenotypes. To understand the
321 roles of *PRX71* and *PRX33* in response to salt stress, we analyzed salt sensitivity and root
322 growth following salt stress or isoxaben treatment in the *prx71-1*, *prx71-2*, and *prx33* loss-of-
323 function mutants, together with *gcn5* and wild-type plants. As observed previously (Figure

324 S1a), under salt stress, the *gcn5* mutant showed reduced survival compared to wild-type plants,
325 whereas the complementation lines showed higher survival than the *gcn5*, partially rescuing
326 the phenotype (Figure 3a, S2a). In contrast, the *prx71* and *prx33* mutants showed statistically
327 higher survival than wild-type plants, and *prx71-2* showed a survival rate comparable to *prx71-*
328 *1* and *prx33* (Figure 3a, S2a). To assess growth responses under salt and cell wall stress, we
329 analyzed the effect of treatment on root length under NaCl and isoxaben treatments (Figure 3b,
330 c). Root lengths were normalized to control conditions in the respective genotype (absolute
331 root lengths are shown in Figure S2b, c). The treatment had a milder effect on root length in
332 the *prx* mutants compared to wild-type. The *gcn5* mutant displayed higher sensitivity, which
333 was restored by GCN5 complementation (Figure 3b, c).

334 We next examined lignin deposition in 10-day-old roots of *gcn5*, *prx71-1*, and *prx33* mutants
335 in response to salt stress. The *gcn5* mutant showed increased lignin deposition after 6 hours of
336 treatment with 150 mM NaCl, including enhanced accumulation in the vasculature and ectopic
337 deposition. In the wild-type roots, lignin accumulation was also observed after 6 hours of
338 treatment, whereas *prx71-1* and *prx33* mutants did not show ectopic lignin deposition. The
339 absence of lignin deposition in *prx71-1* and *prx33* under salt stress suggests that both these
340 peroxidases are critical for lignin deposition during salt-induced cell wall stress (Figure 3d).
341 Together, these results indicate that *PRX71* and *PRX33* contribute to lignin deposition in
342 response to salt stress. Furthermore, the absence of lignin deposition in *prx71-1* and *prx33*
343 mutants correlates with reduced impact of salt treatment on root length, suggesting that lignin
344 accumulation contributes to root growth restriction in response to stress-associated cell wall
345 disruption.

346 **Indirect regulation of *PRX71* and *PRX33* transcription by GCN5 through chromatin**
347 **modification**

348 Given this connection between GCN5, PRX function, and lignin deposition, we next examined
349 whether GCN5 influences *PRX71* and *PRX33* transcription through chromatin modifications.
350 Since *PRX71* and *PRX33* were upregulated in the *gcn5* mutant (Figure 1b), we examined
351 whether this may be reflected in the amount of histone acetylation at the gene loci, in particular
352 at the promoter regions. To this end, we performed chromatin immunoprecipitation (ChIP)
353 assays using an anti-H3K9ac antibody, analyzing histone acetylation at the promoter regions
354 *PRX71* and *PRX33*. Ten-day-old wild-type and *gcn5* seedlings were treated with 150 mM NaCl
355 for 3 hours, at which point we previously observed changes in *PRX* expression (Figure 1b). In
356 line with the histone acetyltransferase function of GCN5, we found reduced H3K9ac

357 enrichment at the promoter regions of *PRX71* and *PRX33* in the *gcn5* mutant compared with
358 wild-type under both control and salt-stress conditions (Figure 4a). In addition, the increase in
359 H3K9ac at *PRX71* upon salt treatment in wild-type was not reflected in *gcn5* (Figure 4a). The
360 increase of H3K9ac at *PRX71* in wild type corresponded with its transcriptional activation upon
361 salt treatment (Figure 1b). However, the expression of *PRX33* and *PRX71* was higher under
362 control (*PRX33*) or salt-treated (*PRX71*) conditions in *gcn5* (Figure 1b) despite the decrease in
363 H3K9ac at both loci in *gcn5*. This suggested that the upregulation of these genes in *gcn5* may
364 be an indirect effect of GCN5 absence. Therefore, we set out to identify potential
365 transcriptional repressors of the PRX genes, hypothesizing that the absence of GCN5 and
366 resulting lower level of H3K9ac at a repressor gene may promote (prime) the transcription of
367 *PRX33* and *PRX71*. Using publicly available transcriptomic and ChIP-seq data, we searched
368 for genes downregulated in *gcn5* that carry less H3K9ac in *gcn5* (Benhamed *et al.* 2008; Wu
369 *et al.* 2023) and that have been identified as direct targets of GCN5 in the wild-type (Kim *et al.*
370 2020; Wu *et al.* 2023) (Figure S3a). Next, we analyzed potential transcription factor binding
371 sites in the promoters of *PRX71* and/or *PRX33* using the Plant Promoter Analysis Navigator
372 (PlantPAN) 4.0 (Chow *et al.* 2024). This analysis identified transcription factors predicted to
373 bind to one or both genes (Table S2). We then compared these transcription factors, predicted
374 to bind the promoters of *PRX71* and *PRX33*, with the list of GCN5-dependent genes identified
375 from transcriptomic and ChIP-seq data (Figure S3b).

376 This led to the identification of transcription factors that could potentially regulate (repress)
377 the *PRX71* and *PRX33* genes in a GCN5-dependent manner, including 16 TFs that were either
378 common to both promoters or specific to either *PRX71* or *PRX33* (Figure S3b, Table S2). We
379 next analyzed the transcript levels of the 16 TFs in wild-type and *gcn5* seedlings under control
380 conditions by qRT–PCR (Figure S3c) and identified three candidates that were differentially
381 expressed in *gcn5* (Figure 4b, S3c). Among these, GATA-type zinc finger transcription factor
382 21 (*GATA21*) was predicted to bind the promoters of both *PRX71* and *PRX33*, whereas MYB-
383 related transcription factor 2 (*MYBS2*) and basic helix-loop-helix 137 *(BHLH137*) were
384 predicted to bind the *PRX33* promoter. *GATA21* and *MYBS2*, but not *BHLH137*, were
385 downregulated in *gcn5*, in line with the requirement of GCN5 for their activation (Figure 4b).
386 We next asked whether the downregulation of these genes in *gcn5* is associated with a loss of
387 H3K9ac. Accordingly, we observed lower enrichment of H3K9ac at the promoters of *GATA21*
388 and *MYBS2* (Figure 4c). Together, these findings suggest that GCN5 may influence *PRX71* and
389 *PRX33* gene expression indirectly through transcription factors such as *GATA21* and *MYBS2*.

390 **Discussion**

391 GCN5 is a subunit of the histone acetyltransferase (HAT) module present in the SAGA and
392 PAGA complexes, where it facilitates histone acetylation, thereby contributing to the
393 regulation of gene expression and numerous plant developmental pathways (Vlachonasios,
394 Thomashow & Triezenberg 2003; Wu *et al.* 2023). Consistent with this central regulatory role,
395 loss of GCN5 function results in smaller rosettes (Vlachonasios *et al.* 2003), short roots and
396 defects in meristem activity (Kornet & Scheres 2009; Servet *et al.* 2010) as well as other
397 developmental defects, and it is associated with altered expression of stress-responsive genes
398 under various environmental stimuli, such as the heat-induced *HSFA3* and *UVH6* (Benhamed
399 *et al.* 2006; Hu *et al.* 2015). Taken together with our results, these studies position GCN5 as a
400 key coordinator of growth and stress adaptation, and our data extend this role to ROS
401 homeostasis and PRX-dependent lignification during salt stress.

402 Notably, recent biochemical and genomic analyses have established that GCN5 operates not
403 only within the conserved SAGA complex (containing ADA2B) but also in a plant-specific
404 complex, named PAGA, which incorporates ADA2A and four additional plant-specific
405 subunits (Wu *et al.* 2023). SAGA and PAGA independently generate high and moderate levels
406 of H3K9 acetylation, respectively, and can antagonistically regulate transcription at shared
407 targets (Wu *et al.* 2023). The *gcn5* mutation eliminates the catalytic subunit shared by both
408 complexes.

409 Thus, the observed reduction in H3K9ac at both PRX and TFs could reflect a combined loss of
410 SAGA and PAGA activity. However, analysis of publicly available ChIP-seq datasets (Wu *et*
411 *al.* 2023) indicates that *PRX71* and *MYBS2* exhibit reduced H3K9ac in *gcn5* and are direct
412 targets bound by the SAGA component ADA2B, supporting a role in this regulatory pathways
413 (Table S3). Nevertheless, disentangling the relative contributions of SAGA and PAGA to PRX
414 regulation, for example, by comparing *ada2a* and *ada2b* single mutants — could reveal
415 whether the indirect regulatory circuit identified here operates primarily through one or both
416 GCN5-containing complexes. Such analysis could also clarify whether the moderate
417 acetylation typically deposited by PAGA is sufficient to maintain expression of the PRX-
418 constraining TFs *GATA21* and *MYBS2* in the absence of SAGA, or whether SAGA-level
419 acetylation is required.

420 Previous research showed that in response to salt stress, TaHAG1, the wheat ortholog of
421 *Arabidopsis* GCN5, helps to maintain ROS balance. In TaHAG1 overexpression lines,

422 cytosolic enzymatic antioxidant activity was increased. However, whether this results from
423 direct gene regulation by TaHAG1 or from its effect on ROS-detoxifying pathways remains
424 unclear (Zheng *et al.* 2021). In hexaploid wheat, TaHAG1 directly induces the expression of
425 respiratory burst oxidase (*Rboh*) genes by promoting H3K9 and H3K14 acetylation at their
426 promoters, resulting in increased NADPH oxidase-dependent ROS production that contributes
427 to Na^+ exclusion and salt tolerance (Zheng *et al.* 2021). By contrast, we observed that loss of
428 Arabidopsis GCN5 led to elevated apoplastic ROS (Figure 1a), driven by class III peroxidases
429 rather than NADPH oxidases. Notably, these findings may reflect compartmentalized ROS
430 management: RBOH-generated superoxide at the plasma membrane might serve as a signaling
431 molecule promoting ion homeostasis, whereas class III PRX-generated H_2O_2 in the apoplast
432 might drive monolignol oxidation and lignin polymerization. In addition, GCN5 contributes to
433 maintaining cell wall integrity under salt stress in Arabidopsis by influencing the expression of
434 genes involved in cellulose synthesis (Zheng *et al.* 2019). Compared with wild-type seedlings,
435 *gcn5* exhibits reduced cellulose content, which is further decreased under salt stress, while
436 lignin accumulation is enhanced together with ectopic lignification (Zheng *et al.* 2019). Our
437 work shows that in response to stress, *gcn5* seedlings accumulated elevated levels of ROS and
438 interestingly, showed altered expression of several class III PRXs. Specifically, we identified
439 *PRX71* and *PRX33* as promising candidates (Figure 1b). Previous studies have shown that in
440 *Arabidopsis*, class III PRXs like *PRX71* limit root elongation (Raggi *et al.* 2015) and
441 overexpression of *AtPRX37* leads to a dwarf phenotype (Pedreira, Herrera, Zarra & Revilla
442 2011), suggesting that altered peroxidase activity may contribute to root growth restriction in
443 *gcn5*. Accordingly, the elevated ROS levels (Figure 1a) and altered *PRX* regulation (Figure 1b,
444 4a) in *gcn5* suggest that a chromatin-level perturbation is translated into a cell wall-centered
445 growth phenotype under salt stress.

446 Lignin deposition is a common response to stress-triggered cell wall damage and is considered
447 to enhance cell wall integrity (Caño-Delgado *et al.* 2003; Denness *et al.* 2011). Class III PRXs
448 are centrally involved in controlling lignin deposition (Cosio & Dunand 2009; Marjamaa *et al.*
449 2009). Enhanced lignin deposition in response to salt stress has been reported in plant species,
450 such as maize (Oliveira *et al.* 2020) and in *Arabidopsis,* showing elevated lignin accumulation
451 (Chun *et al.* 2019). Both *35S::PRX71* and *35S::PRX33* lines exhibited enhanced lignin
452 accumulation similar to the *gcn5* mutant under control conditions. Overall, our data support a
453 role for *PRX71* and *PRX33* in mediating lignification as part of the cell wall reinforcement
454 response. Loss of GCN5 leads to a balance shift towards ROS accumulation and *PRX*-mediated

455 lignification (Figure 1a; Figure 2; Figure 3d). This enhanced lignin deposition correlates with
456 the reduced root growth in response to salt stress (Figure 3b, c). Alternatively, the upregulation
457 of *PRX* expression might be secondary to ROS or cell wall integrity signaling. However, the
458 recapitulation of the enhanced lignification in plants overexpressing *PRX71/PRX33* (Figure 2)
459 suggests that increased PRX abundance and activity are sufficient to drive lignin deposition
460 under non-stress conditions (Figure 2). Together, our results support a functional link between
461 elevated *PRX71*/*PRX33* activity and lignin deposition. Notably, *prx71* and *prx33* loss-of-
462 function mutants showed improved survival under salt stress compared to wild type (Figure
463 3a), suggesting that elevated *PRX*-mediated lignification can be detrimental to salt tolerance.
464 Consistent with this, *prx71* and *prx33* mutants lacked ectopic lignin deposition under salt stress
465 (Figure 3d), supporting a model in which restricting stress-induced lignification is associated
466 with improved survival. Practically, these results suggest that modulating *PRX* activity, or
467 upstream regulators such as GCN5-dependent pathways, may offer a route to improve salt
468 stress resilience in crops.

469 Loss of GCN5 simultaneously reduces cellulose synthesis and derepresses *PRX71/PRX33*
470 expression, promoting ectopic lignin deposition (Zheng *et al.* 2019). Together, these parallel
471 effects point to GCN5 as a chromatin-level switch involved in coordinating the balance
472 between primary (cellulose-based) and secondary (lignin-based) cell wall composition. In
473 wild-type plants under salt stress, GCN5-dependent acetylation likely maintains cellulose
474 production to preserve primary wall integrity while simultaneously limiting compensatory
475 lignification. This balance is disrupted in *gcn5* and the reduced cellulose content could trigger
476 cell wall integrity sensing pathways that amplify *PRX*-mediated lignin deposition, resulting in
477 cell wall stiffening at the cost of growth. In the future, simultaneously restoring cellulose
478 synthesis and suppressing lignification could clarify whether these two arms of the *gcn5* cell
479 wall phenotype are additive or epistatic.

480 While GCN5 is widely recognized for its role in histone acetylation, recent work in *Arabidopsis*
481 has shown that it can also acetylate the transcriptional co-repressor TOPLESS (TPL) and
482 thereby contribute to gene repression. This acetylation promotes interaction of TPL with
483 NOVEL INTERACTOR OF JAZ (NINJA) and its recruitment to target promoters, resulting in
484 chromatin compaction and transcriptional repression (An *et al.* 2022). In our study, reduced
485 H3K9ac enrichment at the *PRX71* and *PRX33* promoter regions in the *gcn5* mutant argues
486 against a simple model in which GCN5 directly activates these PRX loci (Figure 4a). Instead,
487 our findings suggest that GCN5 indirectly regulates *PRX71* and *PRX33*, potentially through

488 transcription factors such as *MYBS2* and *GATA21* (Figure 4b; Figure S3c). This model is
489 consistent with our observation that H3K9ac is reduced at *PRX* promoters (Figure 4a) while
490 *PRX71/PRX33* transcript abundance is elevated (Figure 1b), implying an indirect regulatory
491 route rather than direct activation. However, genome-wide analysis has shown that loss of
492 GCN5 leads to changes in H3K14ac enrichment along genes, with decreased H3K14ac at 5′
493 regions for GCN5 target genes but increased enrichment toward the 3′ ends of upregulated
494 genes. Changes in H3K9ac closely follow those observed for H3K14ac along genes (Kim *et*
495 *al.* 2020). Such changes in histone mark distribution could potentially influence H3K9ac at
496 *PRX* loci and contribute to their transcriptional upregulation in *gcn5*, in parallel with the TF-
497 mediated pathway. Evidence from rice supports a repressive role for *MYBS2*, as reduced
498 *MYBS2* expression leads to elevated *αAmy* gene induction under abiotic stress conditions and
499 improved stress tolerance (Chen *et al.* 2019). A similar model has been reported previously, in
500 which GCN5 limits salicylic acid mediated responses by promoting the expression of genes
501 that act as negative regulators of salicylic acid biosynthesis (Kim *et al.* 2020), suggesting that
502 GCN5 may control biotic stress responses through induction of negative regulators. Together,
503 these observations support a working model in which GCN5 maintains an acetylation-
504 dependent transcriptional program that supports expression of *PRX* constraining TFs, thereby
505 limiting stress-associated lignification and its growth trade-offs under salt stress (Figure 5). In
506 the absence of GCN5, reduced H3K9ac at TF loci may lower TF abundance, relieving
507 repression on *PRX71/PRX33* and promoting lignin deposition. This regulatory model is
508 summarized in Figure 5. In wild type, *GCN5* promotes H3K9ac at loci encoding *PRX*,
509 regulating transcription factors (*GATA21* and *MYBS2*), maintaining their expression. These
510 TFs repress *PRX33*/*PRX71*, thereby limiting *PRX*-driven lignin deposition. In the *gcn5* mutant,
511 reduced H3K9ac is associated with decreased TF expression, relieving repression of
512 *PRX71*/*PRX33* and resulting in elevated PRX abundance and enhanced lignin deposition
513 (Figure 5). This model provides an explanation for the apparent disconnect between reduced
514 H3K9ac at *PRX* promoters (Figure 4a) and increased *PRX71*/*PRX33* transcript abundance
515 (Figure 1b), and it is consistent with the ability of *PRX71/PRX33* overexpression to drive
516 lignification under non-stress conditions (Figure 2) and with reduced salt-associated lignin
517 deposition in *prx* mutants (Figure 3d).

518 Future experiments that directly test causality, for example, genetic epistasis between *gcn5* and
519 *prx33/prx71*, quantitative ROS and lignin measurements beyond staining, and functional
520 validation of *GATA21/MYBS2* at *PRX* promoters, will be important to distinguish primary

521 chromatin-mediated effects from downstream stress responses and to refine the regulatory
522 hierarchy. More broadly, these approaches will help clarify the contribution of *PRX71/PRX33*
523 to the *gcn5* phenotype and their potential role in ROS and cell wall integrity signaling under
524 salt stress.

525

526 **Acknowledgements**

527 This work was supported by the Czech Science Foundation grant No. 22-17092S (PK and
528 MW). We thank Dr. Fatemeh Aflaki for help with ChIP-qPCR, Adam Zeiner for valuable
529 advice on physiological experiments, Media Kitchen (Tomas Kocabek) and the Growth
530 Facility (Jan Kadlec), BC Core Facilities, Institute for Plant Molecular Biology, Biology Centre
531 CAS.

532

533 **Competing interests**

534 The authors declare no competing interests.

535

536 **Author contributions**

537 MS, PK, IM and MW conceived the study and designed the research. MS and JM carried out
538 the work. MS, JM, PK, IM and MW analyzed the data. MS wrote the first draft. All authors
539 edited the final draft of the paper. PK and MW acquired funding for the research.

540

541 **Data availability**

542 Data, plasmids and transgenic plant seeds generated for this study are available upon request
543 from Michael Wrzaczek.

544

545

546 **References**

547 Alonso J.M., Stepanova A.N., Leisse T.J., Kim C.J., Chen H., Shinn P., … Ecker J.R. (2003)
548 Genome-Wide Insertional Mutagenesis of *Arabidopsis thaliana*. *Science* **301**, 653–657.
549 An C., Deng L., Zhai H., You Y., Wu F., Zhai Q., … Li C. (2022) Regulation of jasmonate
550 signaling by reversible acetylation of TOPLESS in *Arabidopsis*. *Molecular Plant* **15**, 1329–
551 1346.
552 Arnaud D., Lee S., Takebayashi Y., Choi D., Choi J., Sakakibara H. & Hwang I. (2017)
553 Cytokinin-Mediated Regulation of Reactive Oxygen Species Homeostasis Modulates Stomatal
554 Immunity in *Arabidopsis*. *The Plant Cell* **29**, 543–559.
555 Baxter A., Mittler R. & Suzuki N. (2014) ROS as key players in plant stress signalling. *Journal*
556 *of Experimental Botany* **65**, 1229–1240.
557 Benhamed M., Bertrand C., Servet C. & Zhou D.-X. (2006) *Arabidopsis GCN5*, *HD1*, and
558 *TAF1/HAF2* interact to regulate histone acetylation required for light-responsive gene
559 expression. *The Plant Cell* **18**, 2893–2903.
560 Benhamed M., Martin-Magniette M., Taconnat L., Bitton F., Servet C., De Clercq R., … Hilson
561 P. (2008) Genome-scale *Arabidopsis* promoter array identifies targets of the histone
562 acetyltransferase GCN5. *The Plant Journal* **56**, 493–504.
563 Bischoff V., Cookson S.J., Wu S. & Scheible W.-R. (2009) Thaxtomin A affects CESA-
564 complex density, expression of cell wall genes, cell wall composition, and causes ectopic
565 lignification in *Arabidopsis thaliana* seedlings. *Journal of Experimental Botany* **60**, 955–965.
566 Boudsocq M. & Sheen J. (2013) CDPKs in immune and stress signaling. *Trends in Plant*
567 *Science* **18**, 30–40.
568 Boyce C.K., Zwieniecki M.A., Cody G.D., Jacobsen C., Wirick S., Knoll A.H. & Holbrook
569 N.M. (2004) Evolution of xylem lignification and hydrogel transport regulation. *Proceedings*
570 *of the National Academy of Sciences* **101**, 17555–17558.
571 Caño-Delgado A., Penfield S., Smith C., Catley M. & Bevan M. (2003) Reduced cellulose
572 synthesis invokes lignification and defense responses in *Arabidopsis thaliana*. *The Plant*
573 *Journal* **34**, 351–362.
574 Chen Y.-S., David Ho T.-H., Liu L., Lee D.H., Lee C.-H., Chen Y.-R., … Yu S.-M. (2019)
575 Sugar starvation-regulated MYBS2 and 14-3-3 protein interactions enhance plant growth,
576 stress tolerance, and grain weight in rice. *Proceedings of the National Academy of Sciences*
577 **116**, 21925–21935.
578 Chow C.-N., Yang C.-W., Wu N.-Y., Wang H.-T., Tseng K.-C., Chiu Y.-H., … Chang W.-C.
579 (2024) PlantPAN 4.0: updated database for identifying conserved non-coding sequences and

exploring dynamic transcriptional regulation in plant promoters. *Nucleic Acids Research* **52**, D1569–D1578.

Chun H.J., Baek D., Cho H.M., Lee S.H., Jin B.J., Yun D.-J., … Kim M.C. (2019) Lignin biosynthesis genes play critical roles in the adaptation of *Arabidopsis* plants to high-salt stress. *Plant Signaling & Behavior* **14**, 1625697.

Colina F.J., Krasensky-Wrzaczek J., Pérez-Guillén A. & Wrzaczek M. (2026) CRK2 modulates flowering in *Arabidopsis* together with GLYCINE-RICH RNA-BINDING PROTEIN 7. *New Phytologist*, nph.70901.

Cosgrove D.J. (2005) Growth of the plant cell wall. *Nature Reviews Molecular Cell Biology* **6**, 850–861.

Cosgrove D.J. (2016) Plant cell wall extensibility: connecting plant cell growth with cell wall structure, mechanics, and the action of wall-modifying enzymes. *Journal of Experimental Botany* **67**, 463–476.

Cosio C. & Dunand C. (2009) Specific functions of individual class III peroxidase genes. *Journal of Experimental Botany* **60**, 391–408.

Czechowski T., Stitt M., Altmann T., Udvardi M.K. & Scheible W.-R. (2005) Genome-wide identification and testing of superior reference genes for transcript normalization in *Arabidopsis*. *Plant Physiology* **139**, 5–17.

Daudi A., Cheng Z., O'Brien J.A., Mammarella N., Khan S., Ausubel F.M. & Bolwell G.P. (2012) The Apoplastic Oxidative Burst Peroxidase in *Arabidopsis* Is a Major Component of Pattern-Triggered Immunity. *The Plant Cell* **24**, 275–287.

Davidson R.S., Choudhury H., Origgi S., Castellan A., Trichet V. & Capretti G. (1995) The reaction of phloroglucinol in the presence of acid with lignin-containing materials. *Journal of Photochemistry and Photobiology A: Chemistry* **91**, 87–93.

De Smet B., Yang X., Plskova Z., Castell C., Fernández-Fernández A., Dard A., … Van Breusegem F. (2025) The nuclear sulfenome of *Arabidopsis*: spotlight on histone acetyltransferase GCN5 regulation through functional thiols. *Journal of Experimental Botany* **76**, 1569–1584.

Denness L., McKenna J.F., Segonzac C., Wormit A., Madhou P., Bennett M., … Hamann T. (2011) Cell wall damage-induced lignin biosynthesis is regulated by a reactive oxygen species- and jasmonic acid-dependent process in *Arabidopsis*. *Plant Physiology* **156**, 1364–1374.

Ding Y., Fromm M. & Avramova Z. (2012) Multiple exposures to drought "train" transcriptional responses in *Arabidopsis*. *Nature Communications* **3**, 740.

613 Fernández-Pérez F., Pomar F., Pedreño M.A. & Novo-Uzal E. (2015) The suppression of
614 AtPRX52 affects fibers but not xylem lignification in *Arabidopsis* by altering the proportion
615 of syringyl units. *Physiologia Plantarum* **154**, 395–406.
616 Gutierrez R., Lindeboom J.J., Paredez A.R., Emons A.M.C. & Ehrhardt D.W. (2009)
617 *Arabidopsis* cortical microtubules position cellulose synthase delivery to the plasma membrane
618 and interact with cellulose synthase trafficking compartments. *Nature Cell Biology* **11**, 797–
619 806.
620 Hamann T. (2015) The Plant Cell Wall Integrity Maintenance Mechanism—Concepts for
621 Organization and Mode of Action. *Plant and Cell Physiology* **56**, 215–223.
622 Hu Z., Song N., Zheng M., Liu X., Liu Z., Xing J., … Sun Q. (2015) Histone acetyltransferase
623 GCN5 is essential for heat stress-responsive gene activation and thermotolerance in
624 *Arabidopsis*. *The Plant Journal* **84**, 1178–1191.
625 Jalmi S.K. & Sinha A.K. (2015) ROS mediated MAPK signaling in abiotic and biotic stress-
626 striking similarities and differences. *Frontiers in Plant Science* **6**.
627 Karimi M., De Meyer B. & Hilson P. (2005) Modular cloning in plant cells. *Trends in Plant*
628 *Science* **10**, 103–105.
629 Kim S., Piquerez S.J.M., Ramirez-Prado J.S., Mastorakis E., Veluchamy A., Latrasse D., …
630 Benhamed M. (2020) GCN5 modulates salicylic acid homeostasis by regulating H3K14ac
631 levels at the 5′ and 3′ ends of its target genes. *Nucleic Acids Research* **48**, 5953–5966.
632 Kornet N. & Scheres B. (2009) Members of the GCN5 Histone Acetyltransferase Complex
633 Regulate PLETHORA-Mediated Root Stem Cell Niche Maintenance and Transit Amplifying
634 Cell Proliferation in *Arabidopsis*. *The Plant Cell* **21**, 1070–1079.
635 Lämke J. & Bäurle I. (2017) Epigenetic and chromatin-based mechanisms in environmental
636 stress adaptation and stress memory in plants. *Genome Biology* **18**, 124.
637 Ma L., Xing L., Li Z. & Jiang D. (2025) Epigenetic control of plant abiotic stress responses.
638 *Journal of Genetics and Genomics* **52**, 129–144.
639 Marjamaa K., Kukkola E.M. & Fagerstedt K.V. (2009) The role of xylem class III peroxidases
640 in lignification. *Journal of Experimental Botany* **60**, 367–376.
641 Mehdi S., Derkacheva M., Ramström M., Kralemann L., Bergquist J. & Hennig L. (2016) The
642 WD40 domain protein MSI1 functions in a histone deacetylase complex to fine-tune abscisic
643 acid signaling. *The Plant Cell* **28**, 42–54.
644 Mittler R. (2002) Oxidative stress, antioxidants and stress tolerance. *Trends in Plant Science*
645 **7**, 405–410.

646 Moraga F. & Aquea F. (2015) Composition of the SAGA complex in plants and its role in
647 controlling gene expression in response to abiotic stresses. *Frontiers in Plant Science* **6**.
648 Moura J.C.M.S., Bonine C.A.V., De Oliveira Fernandes Viana J., Dornelas M.C. & Mazzafera
649 P. (2010) Abiotic and biotic stresses and changes in the lignin content and composition in
650 Plants. *Journal of Integrative Plant Biology* **52**, 360–376.
651 Mozgová I., Wildhaber T., Liu Q., Abou-Mansour E., L'Haridon F., Métraux J.-P., … Hennig
652 L. (2015) Chromatin assembly factor CAF-1 represses priming of plant defence response
653 genes. *Nature Plants* **1**, 15127.
654 Munns R. & Tester M. (2008) Mechanisms of Salinity Tolerance. *Annual Review of Plant*
655 *Biology* **59**, 651–681.
656 O'Brien J.A., Daudi A., Finch P., Butt V.S., Whitelegge J.P., Souda P., … Bolwell G.P. (2012)
657 A peroxidase-dependent apoplastic oxidative burst in cultured *Arabidopsis* cells functions in
658 MAMP-elicited Defense. *Plant Physiology* **158**, 2013–2027.
659 Oliveira D.M., Mota T.R., Salatta F.V., Sinzker R.C., Končitíková R., Kopečný D., … Dos
660 Santos W.D. (2020) Cell wall remodeling under salt stress: Insights into changes in
661 polysaccharides, feruloylation, lignification, and phenolic metabolism in maize. *Plant, Cell &*
662 *Environment* **43**, 2172–2191.
663 Passardi F., Penel C. & Dunand C. (2004) Performing the paradoxical: how plant peroxidases
664 modify the cell wall. *Trends in Plant Science* **9**, 534–540.
665 Pedreira J., Herrera M.T., Zarra I. & Revilla G. (2011) The overexpression of *AtPrx37*, an
666 apoplastic peroxidase, reduces growth in *Arabidopsis*. *Physiologia Plantarum* **141**, 177–187.
667 Persson S., Paredez A., Carroll A., Palsdottir H., Doblin M., Poindexter P., … Somerville C.R.
668 (2007) Genetic evidence for three unique components in primary cell-wall cellulose synthase
669 complexes in *Arabidopsis*. *Proceedings of the National Academy of Sciences* **104**, 15566–
670 15571.
671 Pradhan Mitra P. & Loqué D. (2014) Histochemical staining of *Arabidopsis thaliana* secondary
672 cell wall elements. *Journal of Visualized Experiments*, 51381.
673 Raggi S., Ferrarini A., Delledonne M., Dunand C., Ranocha P., Lorenzo G.D., … Ferrari S.
674 (2015) The *Arabidopsis* class III peroxidase AtPRX71 negatively regulates growth under
675 physiological conditions and in response to cell wall damage. *Plant Physiology* 169, 2513–
676 2525.
677 Rogers L.A. & Campbell M.M. (2004) The genetic control of lignin deposition during plant
678 growth and development. *New Phytologist* **164**, 17–30.

Sako K., Kim J.-M., Matsui A., Nakamura K., Tanaka M., Kobayashi M., … Seki M. (2016) Ky-2, a Histone Deacetylase Inhibitor, Enhances High-Salinity Stress Tolerance in *Arabidopsis thaliana*. *Plant and Cell Physiology* **57**, 776–783.

Scheible W.-R., Eshed R., Richmond T., Delmer D. & Somerville C. (2001) Modifications of cellulose synthase confer resistance to isoxaben and thiazolidinone herbicides in *Arabidopsis Ixr1* mutants. *Proceedings of the National Academy of Sciences* **98**, 10079–10084.

Servet C., Conde E Silva N. & Zhou D.-X. (2010) Histone Acetyltransferase AtGCN5/HAG1 Is a Versatile Regulator of Developmental and Inducible Gene Expression in Arabidopsis. *Molecular Plant* **3**, 670–677.

Shigeto J., Kiyonaga Y., Fujita K., Kondo R. & Tsutsumi Y. (2013) Putative cationic cell-wall-bound peroxidase homologues in *Arabidopsis*, AtPrx2, AtPrx25, and AtPrx71, are involved in lignification. *Journal of Agricultural and Food Chemistry* **61**, 3781–3788.

Shigeto J. & Tsutsumi Y. (2016) Diverse functions and reactions of class III peroxidases. *New Phytologist* **209**, 1395–1402.

Somerville C., Bauer S., Brininstool G., Facette M., Hamann T., Milne J., … Youngs H. (2004) Toward a systems approach to understanding plant cell walls. *Science* **306**, 2206–2211.

Tariq F., Ma C. & Zhao S. (2025) Integrative dynamics of cell wall architecture and plant growth under salt stress. *Frontiers in Plant Science* **16**, 1644412.

Tenhaken R. (2015) Cell wall remodeling under abiotic stress. *Frontiers in Plant Science* **5**.

Ueda M. & Seki M. (2020) Histone modifications form epigenetic regulatory networks to regulate abiotic stress response. *Plant Physiology* **182**, 15–26.

Vlachonasios K.E., Thomashow M.F. & Triezenberg S.J. (2003) Disruption mutations of *ADA2b* and *GCN5* transcriptional adaptor genes dramatically affect *Arabidopsis* growth, development, and gene expression. *The Plant Cell* **15**, 626–638.

Wu C.-J., Yuan D.-Y., Liu Z.-Z., Xu X., Wei L., Cai X.-W., … He X.-J. (2023) Conserved and plant-specific histone acetyltransferase complexes cooperate to regulate gene transcription and plant development. *Nature Plants* **9**, 442–459.

Wurzinger B., Mair A., Pfister B. & Teige M. (2011) Cross-talk of calcium-dependent protein kinase and MAP kinase signaling. *Plant Signaling & Behavior* **6**, 8–12.

Xia X.-J., Zhou Y.-H., Shi K., Zhou J., Foyer C.H. & Yu J.-Q. (2015) Interplay between reactive oxygen species and hormones in the control of plant development and stress tolerance. *Journal of Experimental Botany* **66**, 2839–2856.

711 Zheng M., Lin J., Liu X., Chu W., Li J., Gao Y., … Hu Z. (2021) Histone acetyltransferase
712 TaHAG1 acts as a crucial regulator to strengthen salt tolerance of hexaploid wheat. *Plant*
713 *Physiology* **186**, 1951–1969.
714 Zheng M., Liu X., Lin J., Liu X., Wang Z., Xin M., … Hu Z. (2019) Histone acetyltransferase
715 GCN5 contributes to cell wall integrity and salt stress tolerance by altering the expression of
716 cellulose synthesis genes. *The Plant Journal* **97**, 587–602.
717

718 **Figure legends:**

719 **Figure 1 Enhanced ROS accumulation and upregulation of *PRX* genes in the *gcn5***
720 **mutant.** (a) DAB staining of 10-day-old wild-type and *gcn5* seedlings after 6 hours of
721 treatment under control conditions, 150 mM NaCl, or with 300 nM isoxaben. Images are
722 representative of at least three independent biological experiments. Scale bar = 0.5 mm. (b)
723 Expression levels of selected PRX genes at different time points during 150 mM NaCl
724 treatment. Transcript levels were normalized to a housekeeping gene and expressed relative to
725 wild type at 0 hour (=1). Data represent mean ± SE of three biological replicates. Statistical
726 significance was determined using two-way ANOVA followed by Tukey's HSD test. Different
727 letters indicate significant differences.

728

729 **Figure 2 *PRX71* and *PRX33* contribute to lignin deposition.** Lignin deposition in roots of
730 wild type, *gcn5* mutant, *prx71* mutant, *prx33* mutant, and *35S::PRX33* and *35S::PRX71*
731 overexpression lines under control conditions. Arrows indicate ectopic lignin deposition.
732 Images are representative of at least three independent biological experiments. Scale bar = 50
733 μm.

734

735 **Figure 3 Salt stress responses and lignin deposition.** (a) Survival rates under salt stress.
736 Survival was calculated relative to plants grown under control conditions. Data represent mean
737 ± SE ($n \geq 3$ biological replicates). Statistical analysis was performed using two-way ANOVA
738 after confirming homogeneity of variance (Levene's test, $p = 0.070$), followed by Tukey's HSD
739 test. Different letters indicate significant differences. (b) Root length was calculated relative to
740 plants grown under control conditions. Primary root length (%) measured at day 12 for
741 seedlings grown on control or 150 mM NaCl containing medium. (c) Primary root length (%)

742 measured at day 12 for seedlings grown on control or 2.5 nM isoxaben containing medium.
743 Root length was calculated relative to plants grown under control conditions. Data in (b) and
744 (c) were analyzed using the Kruskal–Wallis test due to unequal variances (Levene's test, $p <$
745 0.05), followed by the Wilcoxon post-hoc test. Different letters indicate significant differences.
746 Absolute root lengths are shown in Figure S2b and S2c. (d) Lignin deposition in roots of wild
747 type, *gcn5*, *prx71*, and *prx33* mutants after 6 hours of 150 mM NaCl treatment. Arrows indicate
748 ectopic lignin deposition in the *gcn5* mutant. Images are representative of at least three
749 independent experiments. Scale bar = 50 μm.

750

751 **Figure 4 GCN5 indirectly regulates *PRX33* and *PRX71* through chromatin modification**
752 **and transcription factor activity.** (a) ChIP–qPCR analysis of H3K9ac enrichment at the
753 promoter regions of *PRX71* and *PRX33* in wild-type and *gcn5* seedlings under control and 150
754 mM NaCl conditions. ChIP was performed using anti-H3K9ac antibodies, and enrichment was
755 normalized to total H3. A transposable element locus (*At4g03770*) was included as a negative
756 control. Statistical analysis was performed using two-way ANOVA after confirming
757 homogeneity of variance (Levene's test, $p > 0.05$), followed by Tukey's HSD test. (b) Relative
758 expression of candidate transcription factor genes in wild-type and *gcn5* seedlings under
759 control conditions, measured by qRT–PCR. Statistical analysis was performed using a two-
760 tailed Student's t-test. (c) ChIP–qPCR analysis of H3K9ac enrichment at the promoter regions
761 of *GATA21* and *MYBS2* in wild-type and *gcn5* seedlings under control conditions. ChIP was
762 performed using anti-H3K9ac antibodies, and enrichment was normalized to total H3.
763 Statistical analysis was performed using a two-tailed Student's t-test.

764

765 **Figure 5 Proposed model for indirect regulation of *PRX71/PRX33* and lignin deposition**
766 **by GCN5.** In wild type (top), GCN5 promotes H3K9 acetylation (H3K9ac) at loci encoding
767 *PRX* regulating transcription factors (TFs; e.g., *GATA21* and *MYBS2*), maintaining TF
768 expression. These TFs repress *PRX71/PRX33*, thereby limiting *PRX* driven lignin deposition.
769 In the *gcn5* mutant (bottom), reduced H3K9ac is associated with decreased TF expression,
770 relieving repression of *PRX71/PRX33* and resulting in elevated *PRX* activity and enhanced
771 lignin deposition.

772

773 **Supplementary figure legends:**

774 **Supplementary Figure S1** Salt sensitivity and differentially expressed *PRX* genes in the *gcn5*
775 mutant. (a) Survival rates of seedlings after salt treatment. Values are normalized to the
776 corresponding genotype grown under control conditions. Data represent mean ± SE ($n \geq 3$
777 biological replicates). Statistical analysis was performed using two-way ANOVA after
778 confirming homogeneity of variance (Levene's test, $p > 0.05$), followed by Tukey's HSD test.
779 Different letters indicate significant differences. (b) Primary root length (mm) measured at day
780 12 for seedlings grown on control or 150 mM NaCl-containing medium. Statistical analysis
781 was performed using the Kruskal–Wallis test due to unequal variances (Levene's test, $p < 0.05$),
782 followed by the Wilcoxon post-hoc test. Different letters indicate significant differences. (c)
783 Differentially expressed *PRX* genes in the *gcn5* mutant were identified from publicly available
784 transcriptomic data. *PRX/PER* genes belong to class III peroxidases, whereas *GPX* genes
785 encode glutathione peroxidases. (d) Expression levels of differentially expressed *PRX* genes at
786 various time points during 150 mM NaCl treatment. Data represent mean ± SE of two
787 biological replicates. Statistical significance was determined using two-way ANOVA followed
788 by Tukey's HSD test. Different letters indicate significant differences.

789

790 **Supplementary Figure S2** Salt stress responses in *gcn5*, complementation lines, and *prx*
791 mutants. (a) Survival of plants grown on control and NaCl containing media. Scale bar = 1cm.
792 (b) Primary root length (mm) measured at day 12 for seedlings grown on control or 150 mM
793 NaCl containing medium. (c) Primary root length (mm) measured at day 12 for seedlings grown
794 on control or 2.5 nM isoxaben containing medium. Data were analyzed using the Kruskal–
795 Wallis test due to unequal variances (Levene's test, $p < 0.05$), followed by the Wilcoxon post-
796 hoc test. Different letters indicate significant differences.

797

798 **Supplementary Figure S3** Analysis of candidate transcription factors under control
799 conditions. (a) Venn diagrams constructed using publicly available transcriptomic (RNA-seq)
800 and ChIP-seq datasets. In (i), A represents genes downregulated in *gcn5* identified by RNA-
801 seq (Wu *et al.* 2023), B represents genes showing reduced H3K9ac enrichment in *gcn5*
802 identified by ChIP-seq (Wu *et al.* 2023), and C represents GCN5 target genes identified in
803 wild-type plants by ChIP-seq (Kim *et al.* 2020). In (ii), D represents genes downregulated in
804 *gcn5* identified by RNA-seq (Benhamed *et al.* 2008), E represents genes showing reduced

805 H3K9ac enrichment in *gcn5* identified by ChIP-seq (Wu *et al.* 2023), and F represents GCN5
806 target genes identified in wild-type plants by ChIP-seq (Kim *et al.* 2020). In (iii), G represents
807 genes downregulated in *gcn5* identified by RNA-seq (Wu *et al.* 2023), H represents genes
808 showing reduced H3K9ac enrichment in *gcn5* identified by ChIP-seq (Wu *et al.* 2023), and I
809 represents GCN5 target genes identified in wild-type plants by ChIP-seq (Wu *et al.* 2023). A
810 downward arrow (↓) indicates lower enrichment. (b) Venn diagrams comparing transcription
811 factor binding sites (TFBS) of the PRX71 (upper row) and PRX33 (lower row) promoters with
812 overlapping gene sets from (a) i–iii. Letter combinations (e.g., B ∩ C, A ∩ B, E ∩ F) indicate
813 intersections between the gene sets identified in (a) i–iii. Only combinations with at least one
814 common gene are shown. Combinations with zero overlapping genes were observed but not
815 shown above. TFs obtained from the gene set intersections were compiled. After removing
816 duplicates, 16 TFs were selected for further analysis. These TFs include those shared between
817 the PRX71 and PRX33 promoters, as well as those specific to either promoter. (c) Expression
818 levels of differentially expressed transcription factor genes under control conditions measured
819 by qRT–PCR. Data represent mean ± SD of three biological replicates. Statistical significance
820 was determined using a two-tailed Student's t-test.
821

822 **Supplementary Figure S4** Confirmation of T-DNA mutant (a) Genomic DNA from Col-0 and
823 mutant plants was used as a template for PCR to confirm the presence of T-DNA insertion
824 lines. (b) RT-PCR analysis showed the absence of transcript in the mutants. *GCN5* specific
825 primers were used in lanes 1 and 2, *PRX71-1* specific primers in lanes 6 and 7, *PRX71-2*
826 specific primers in lanes 11 and 12, and *PRX33* primers in lanes 16 and 17. *PP2AA3* was used
827 as an internal reference for all samples (lanes 3, 4, 8, 9, 13, 14, 18, and 19).

828

829 **Supplementary Table S1** Primer sequences used for all experimental analyses.

830 **Supplementary Table S2** Potential transcription factor binding sites in the promoters of
831 *PRX71* and *PRX33*.

832 **Supplementary Table S3** Differentially expressed genes (DEGs) and ChIP peak changes in
833 selected genes.

834

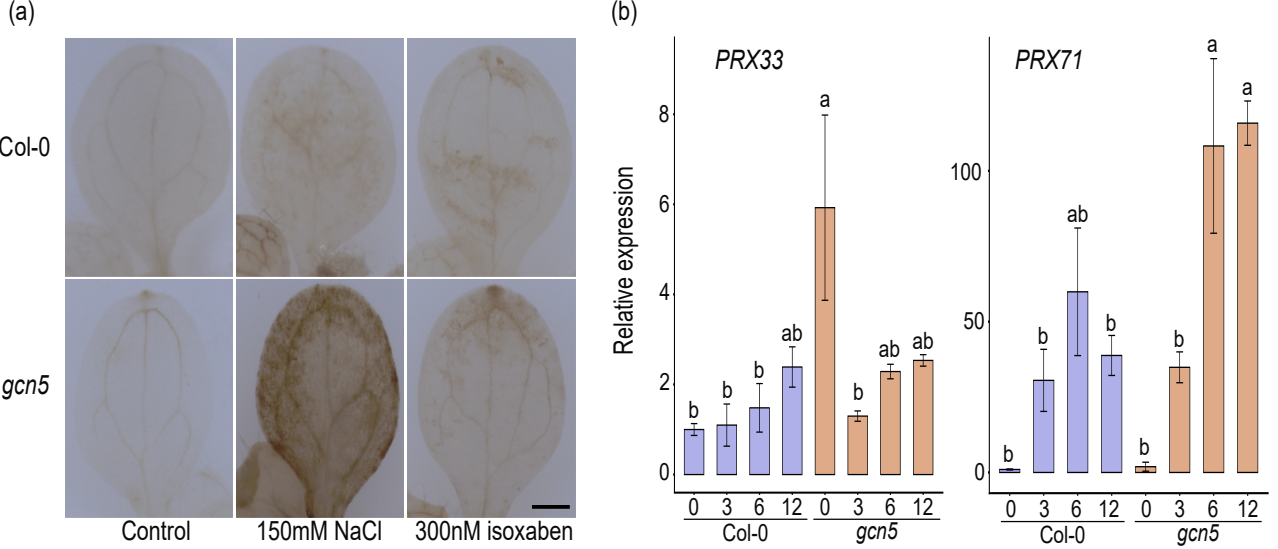

Figure 1 Enhanced ROS accumulation and upregulation of *PRX* genes in the *gcn5* mutant. (a) DAB staining of 10-day-old wild-type and *gcn5* seedlings after 6 hours of treatment under control conditions, 150 mM NaCl, or with 300 nM isoxaben. Images are representative of at least three independent biological experiments. Scale bar = 0.5 mm. (b) Expression levels of selected *PRX* genes at different time points during 150 mM NaCl treatment. Transcript levels were normalized to a housekeeping gene and expressed relative to wild type at 0 hour (=1). Data represent mean ± SE of three biological replicates. Statistical significance was determined using two-way ANOVA followed by Tukey's HSD test. Different letters indicate significant differences.

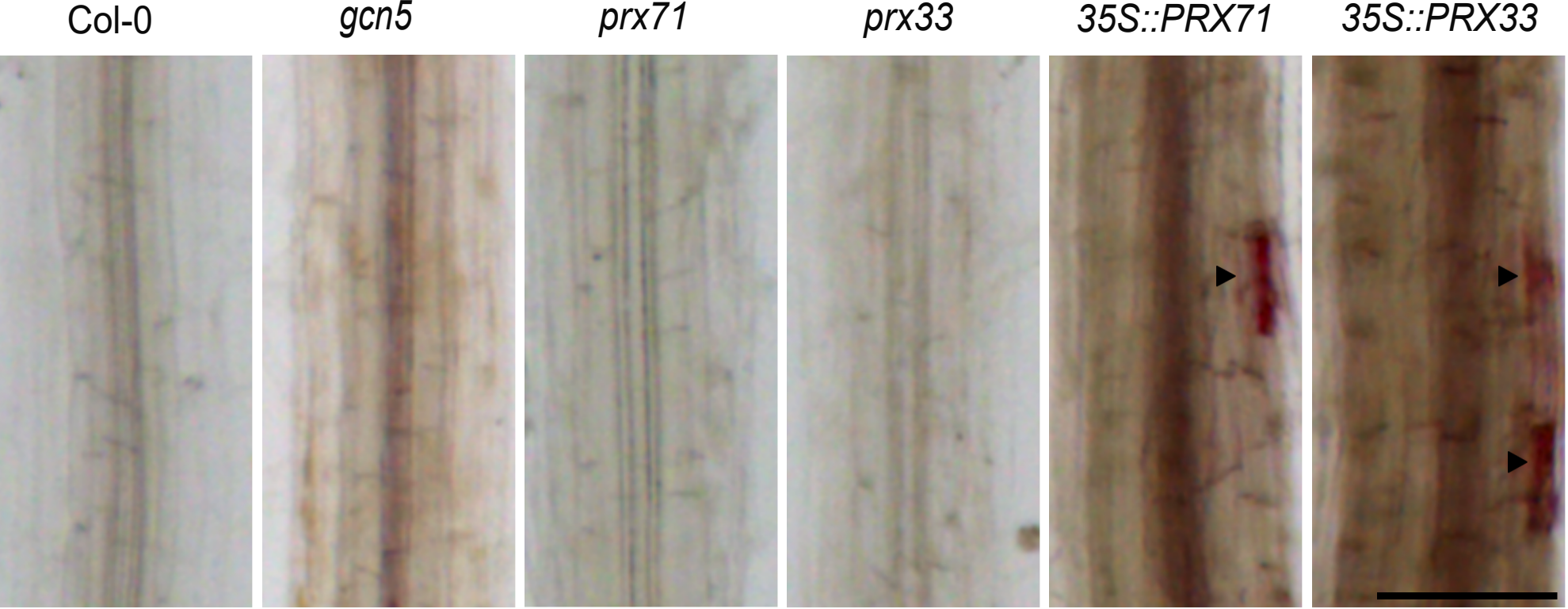

Figure 2 *PRX33* and *PRX71* contribute to lignin deposition. Lignin deposition in roots of wild type, *gcn5* mutant, *prx71* mutant, *prx33* mutant, and *35S::PRX33* and *35S::PRX71* overexpression lines under control conditions. Arrows indicate ectopic lignin deposition. Images are representative of at least three independent biological experiments. Scale bar = 50 μm.

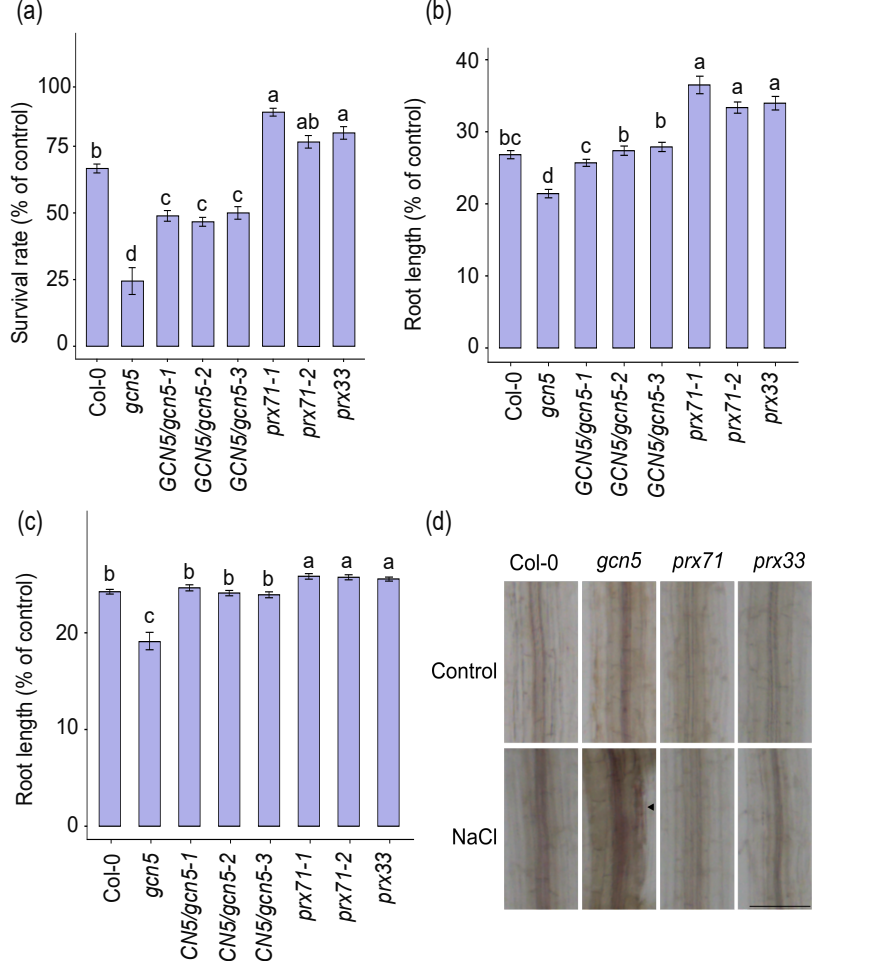

Figure 3 Salt stress responses and lignin deposition. (a) Survival rates under salt stress. Survival was calculated relative to plants grown under control conditions. Data represent mean ± SE (n ≥ 3 biological replicates). Statistical analysis was performed using two-way ANOVA after confirming homogeneity of variance (Levene's test, p = 0.070), followed by Tukey's HSD test. Different letters indicate significant differences. (b) Root length was calculated relative to plants grown under control conditions. Primary root length (%) measured at day 12 for seedlings grown on control or 150 mM NaCl containing medium. (c) Primary root length (%) measured at day 12 for seedlings grown on control or 2.5 nM isoxaben containing medium. Root length was calculated relative to plants grown under control conditions. Data in (b) and (c) were analyzed using the Kruskal–Wallis test due to unequal variances (Levene's test, p < 0.05), followed by the Wilcoxon post-hoc test. Different letters indicate significant differences. Absolute root lengths are shown in Figure S2b and S2c. (d) Lignin deposition in roots of wild type, *gcn5*, *prx71*, and *prx33* mutants after 6 hours of 150 mM NaCl treatment. Arrows indicate ectopic lignin deposition in the *gcn5* mutant. Images are representative of at least three independent experiments. Scale bar = 50 µm.

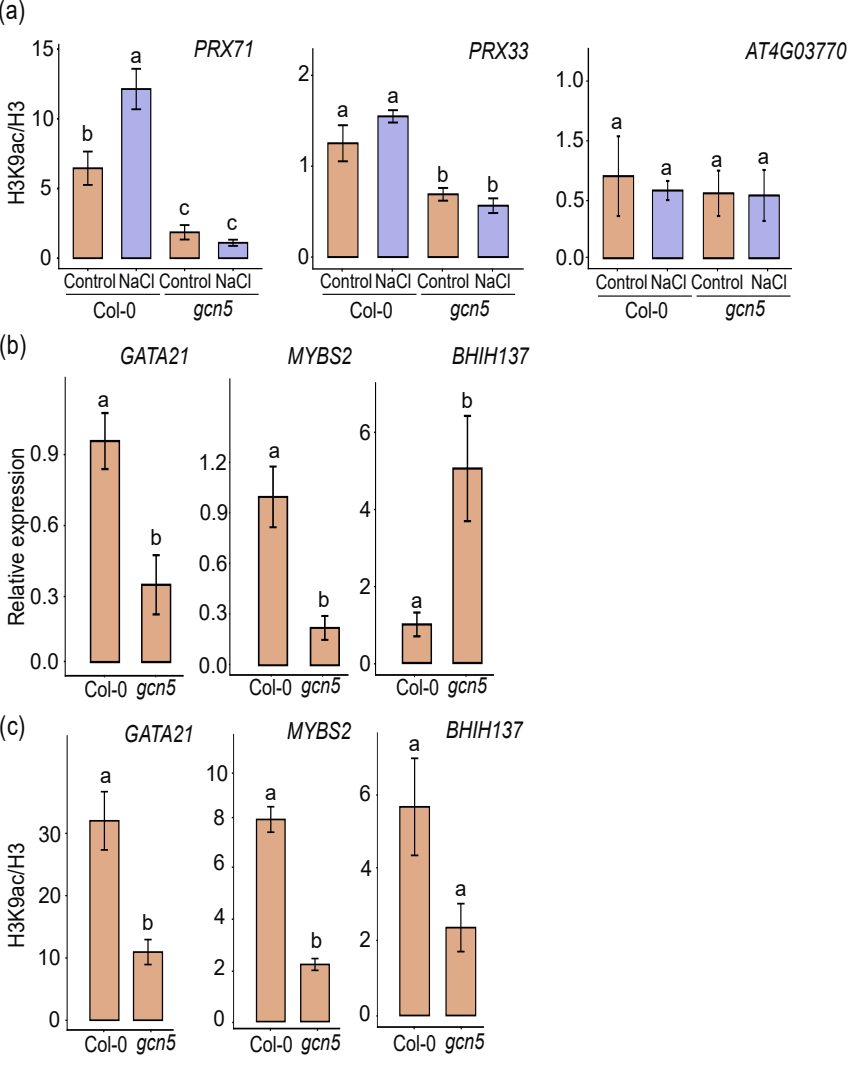

Figure 4 GCN5 indirectly regulates *PRX33* and *PRX71* through chromatin modification and transcription factor activity. (a) ChIP–qPCR analysis of H3K9ac enrichment at the promoter regions of *PRX71* and *PRX33* in wild-type and *gcn5* seedlings under control and 150 mM NaCl conditions. ChIP was performed using anti-H3K9ac antibodies, and enrichment was normalized to total H3. A transposable element locus (*At4g03770)* was included as a negative control. Statistical analysis was performed using two-way ANOVA after confirming homogeneity of variance (Levene's test, $p > 0.05$), followed by Tukey's HSD test. (b) Relative expression of candidate transcription factor genes in wild-type and *gcn5* seedlings under control conditions, measured by qRT–PCR. Statistical analysis was performed using a two-tailed Student's t-test. (c) ChIP–qPCR analysis of H3K9ac enrichment at the promoter regions of *GATA21* and *MYBS2* in wild-type and *gcn5* seedlings under control conditions. ChIP was performed using anti-H3K9ac antibodies, and enrichment was normalized to total H3. Statistical analysis was performed using a two-tailed Student's t-test.

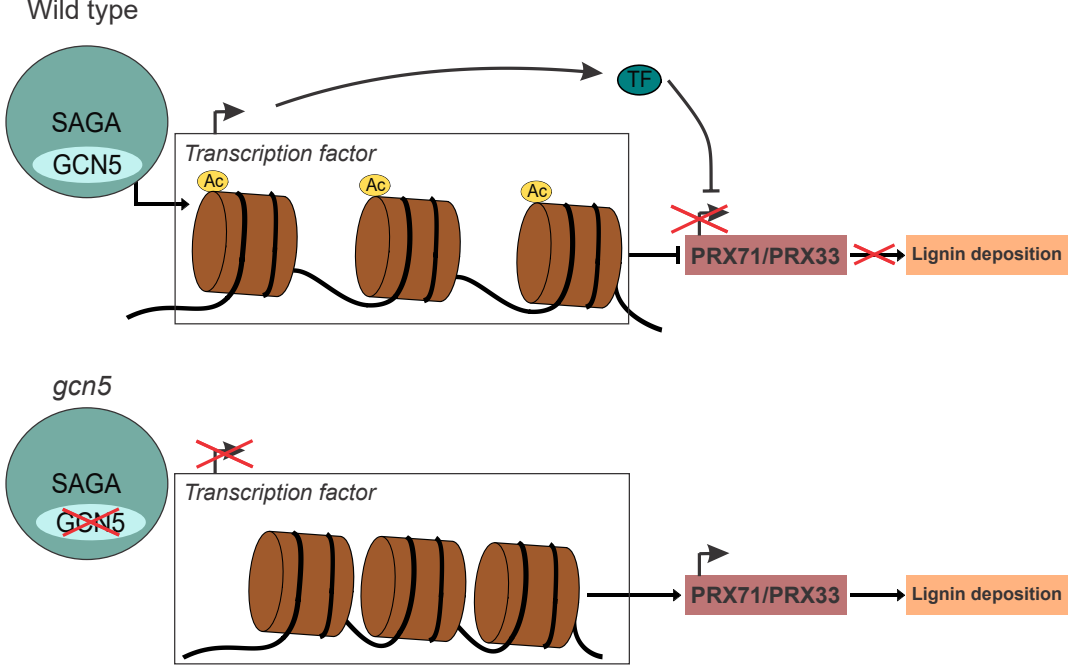

Figure 5 Proposed model for indirect regulation of *PRX71/PRX33* and lignin deposition by GCN5. In wild type (top), GCN5 promotes H3K9 acetylation (H3K9ac) at loci encoding *PRX* regulating transcription factors (TFs; e.g., *GATA21* and *MYBS2*), maintaining TF expression. These TFs repress *PRX71/PRX33*, thereby limiting *PRX* driven lignin deposition. In the *gcn5* mutant (bottom), reduced H3K9ac is associated with decreased TF expression, relieving repression of *PRX71/PRX33* and resulting in elevated *PRX* activity and enhanced lignin deposition.